Article

Tailored Emission Spectrum of 2D Semiconductors Using Plasmonic Nanocavities

Jiani Huang,[†] Gleb M. Akselrod,[‡] Tian Ming,[§] Jing Kong,[§] and Maiken H. Mikkelsen[*,†,‡]

[†]Department of Physics, Duke University, Durham, North Carolina 27708, United States

[‡]Department of Electrical and Computer Engineering, Duke University, Durham, North Carolina 27708, United States

[§]Department of Electrical Engineering and Computer Science, Massachusetts Institute of Technology, Cambridge, Massachusetts 02139, United States

ABSTRACT: Tailoring light−matter interactions in monolayer MoS_2 is critical for its use in optoelectronic and nanophotonic devices. While significant effort has been devoted to enhancing the photoluminescence intensity in monolayer MoS_2, tailoring of the emission spectrum including complex excitonic states remains largely unexplored. Here, we demonstrate that the peak emission wavelengths of the A and B excitons can be tuned up to 40 and 25 nm, respectively, by integrating monolayer MoS_2 into a plasmonic nanocavity with tunable plasmon resonances. Contrary to the intrinsic photoluminescence spectrum of monolayer MoS_2, we are also able to create a dominant B exciton peak when the nanocavity is resonant with its emission. Additionally, we observe a 1200-fold enhancement of the A exciton emission and a 6100-fold enhancement of the B exciton emission when normalized to the area under a single nanocavity and compared to a control sample on thermal oxide.

KEYWORDS: plasmonics, nanocavity, MoS_2, exciton, photoluminescence enhancement, B exciton
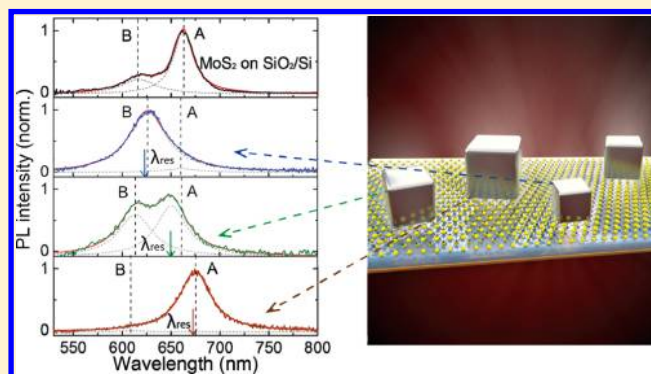
Monolayer molybdenum disulfide (MoS_2) offers an appealing platform for applications in nanophotonics and optoelectronics due to its remarkable optical properties.[1,2] Owing to its atomically thin layer, monolayer MoS_2 can be easily integrated with other low-dimensional materials such as quantum dots,[3] nanowires,[4,5] and other 2D materials[6,7] to form hybrid nanostructures with intriguing optical and electronic properties. Monolayer MoS_2 has also been demonstrated to have tightly bound excitons due to the reduced dielectric screening effect;[8] hence, the excitons remain stable even at room temperature. In addition to neutral excitons, monolayer MoS_2 possesses a variety of more complex exciton states such as charged excitons (trions), biexcitons, and bound-excitons. The origin and dynamics of these excitonic states, as well as experimental manipulation, have been widely explored.[9−17] Among the various exciton species, the A and B excitons (each having neutral and trion states) have attracted considerable research interest.

In monolayer MoS_2, an inversion symmetry breaking combined with a strong spin−orbit coupling results in a large valence band splitting of ~150 meV at the ±K points in the first Brillouin zone.[18] As illustrated in Figure 1a, this energy splitting gives rise to two different valley exciton species, namely the A and B excitons, which are associated with the optical transitions from the upper and the lower valence band to the bottom of the conduction band, respectively. These two excitons are manifested as the dominant peaks in the room-temperature

absorption and emission spectra of monolayer MoS_2, and hence are predicted to play a crucial role in the operation of future optoelectronic devices. However, compared to other direct band gap semiconductors, monolayer MoS_2 suffers from weak light absorption and low photoluminescence (PL) quantum yield partly due to its subnanometer thin layer. The absolute PL quantum yield is observed to be 0.4% for suspended monolayers.[2] The main contribution to this value is from the dominant A exciton emission, while the B exciton emission is much weaker with PL intensity of ~20% of the A exciton emission.[19] Due to the lower intrinsic quantum yield of the B exciton emission, it has not been explored for use in optoelectronic or nanophotonic devices. Thus, enhancing the B exciton emission provides flexibility for choosing the operating wavelength of future devices as well as provides an avenue for reconfigurable structures and devices operating at multiple wavelengths simultaneously.

To date, a large variety of strategies have been explored to enhance the optical absorption and emission in monolayer MoS_2,[4,5,19−30] such as chemical treatment[29], nanostructuring of monolayers,[27] using photonic crystal cavities[30] and incorporation of nanowires.[4,5] Among these methods, a promising approach is the integration of monolayers with plasmonic nanostructures. Plasmonic systems have been widely used to
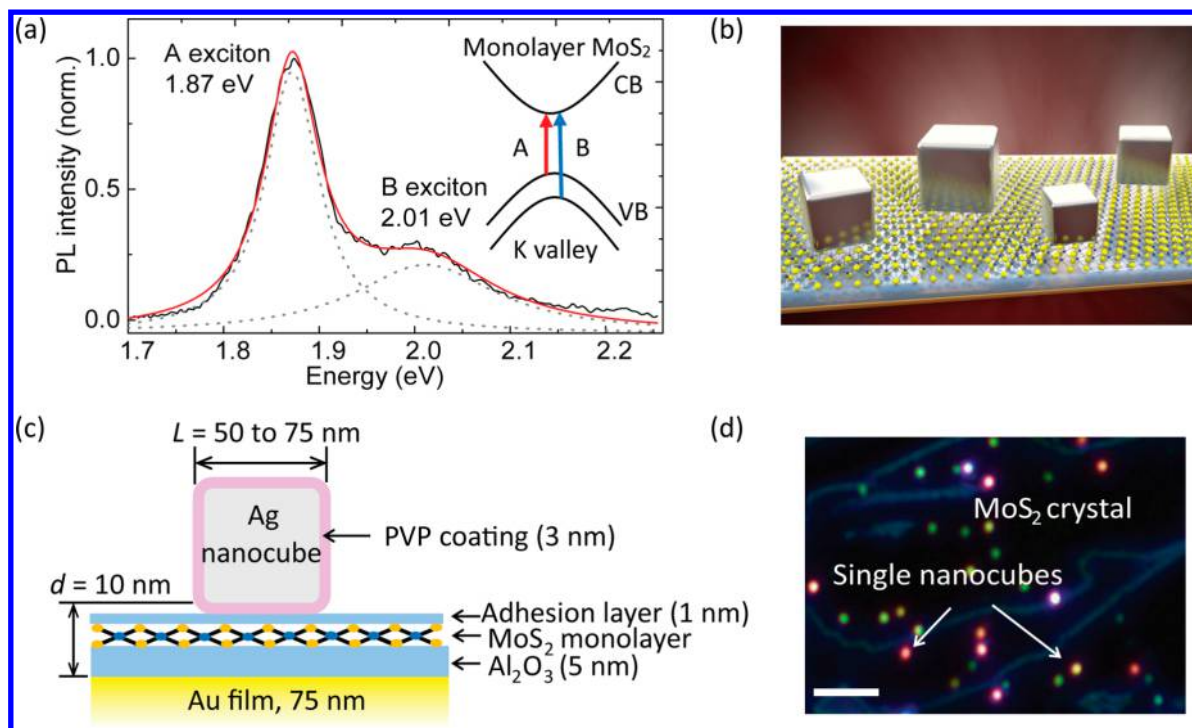
Figure 1. Sample schematic and characterization. (a) Normalized PL spectrum of monolayer MoS_2 control sample on SiO_2/Si substrate. The measured spectrum (black line) was fitted to A and B exciton peaks at 1.87 and 2.01 eV, respectively (dashed lines). Inset: a schematic band structure of monolayer MoS_2 in the K valley, showing the optical transitions associated with the A and B excitons. CB: conduction band; VB: valence band. (b) 3D illustration of the plasmonic nanocavity, consisting of silver nanocubes of varying sizes on top of a gold film, separated by an Al_2O_3 layer, a MoS_2 monolayer, and a polyelectrolyte adhesion layer. (c) Schematic illustration of the fabricated nanocavity sample. (d) Dark-field microscope image of the fabricated sample. The edges of MoS_2 monolayer appear as the blue outlines and the bright spots represent individual nanocavities. The scale bar is 5 μm.

tailor nanoscale light−matter interactions such as enabling surface-enhanced Raman scattering,[31] facilitating nonlinear optical processes,[32] and achieving enhanced fluorescence.[33,34] Relying on the use of localized surface plasmon resonances, their capability of confining light in a subwavelength volume can strongly boost optical processes such as light absorption and emission at the nanoscale.

Various plasmonic nanostructures have previously been used to enhance the PL in 2D transition metal dichalcogenides such as monolayer MoS_2, including core−shell gold nanoparticles,[21] silver nanodisk arrays,[22] silver bowtie arrays,[23] and gold nanorods[24,25] with enhancements of 2−60-fold. Recently using film-coupled silver nanocubes, PL enhancements up to 2,000-fold has been observed in monolayer MoS_2 when normalized to the area under a single nanocube.[19] However, less effort has been denoted to tailoring the emission spectrum and probing the relationship between the nanocavity resonance and the PL enhancement factor. Additionally, previous work has focused on the enhancement of the A exciton emission and, in some cases, as a side effect observed a limited 2−25-fold enhancement in the B exciton emission.[23,26]

In this work, we utilize colloidally synthesized plasmonic nanocavities based on a film-coupled nanopatch antenna design,[19] which is illustrated in Figure 1b,c. This particular plasmonic nanocavity possesses an ultrasmall effective mode volume of $\approx 0.001(\lambda/n)^3$; hence, the electromagnetic field is well confined in the sub-10 nm gap, achieving large field enhancements.[33−35] Additionally, the plasmon resonance can be tuned by varying either the gap thickness or the nanocube size,[36] which makes this nanocavity promising to enhance the

intrinsically weakly emitting B exciton by overlapping the nanocavity resonance with the B exciton peak. Here, we demonstrate tunable emission wavelengths of the A and B exciton in monolayer MoS_2 by tuning the plasmonic nanocavity resonance across the emission spectrum. The shape and position of both exciton peaks are strongly modified when coupled to the plasmonic nanocavity, exhibiting a correlation between the nanocavity resonance and the emission peak wavelengths. Furthermore, we also observe a 6100-fold enhancement of the B exciton emission and a 1200-fold enhancement of the A exciton emission relative to a control sample consisting of the monolayer on thermal oxide. Compared to the free space PL spectrum which is dominated by the A exciton peak, we are capable of achieving a dominant B exciton emission by overlapping the plasmon resonance with the B exciton energy.

The geometry of the plasmonic nanocavity that we utilize is illustrated in Figure 1b,c. The structure is fabricated by first evaporating a 75 nm gold film on top of a silicon substrate. Then 5 nm of Al_2O_3, which acts as a dielectric spacer layer, is deposited on the gold using atomic layer deposition (ALD). After that, monolayer MoS_2 grown by chemical vapor deposition (CVD) is transferred onto the Al_2O_3 layer, followed by the deposition of a 1 nm polyelectrolyte adhesion layer and colloidal silver nanocubes. The nanocubes have a range of sizes, L, from 50 to 75 nm, as labeled in Figure 1c, including a 3 nm poly(vinylpyrrolidinone) (PVP) coating around the nanocubes, which is a byproduct of the nanocube synthesis. The density of the deposited nanocubes is sufficiently low to allow optical measurements of individual nanocubes. The total gap thickness

d in this nanostructure is ~10 nm, which consists of a 5 nm Al_2O_3 layer, a MoS_2 monolayer (~0.7 nm), a 1 nm adhesion layer, and the 3 nm PVP coating. Additionally, a control sample of monolayer MoS_2 on a thermal oxide SiO_2 (300 nm)/Si substrate is also fabricated.

As a reference, we first measured the intrinsic PL spectrum from the control sample, as shown in Figure 1a. The spectrum can be fitted to two Lorentz-shaped peaks, corresponding to the A and B excitons at 1.87 and 2.01 eV, respectively. Their associated optical transitions in the K valley are illustrated in the inset in Figure 1a. We should note that, in the broad room-temperature emission spectrum, it is difficult to distinguish the A exciton and A trion peaks, as they are only ~20 meV apart.[37] Thus, we fit all the PL spectra in this work to two Lorentz-shaped A and B exciton peaks.

For the nanocavity sample, individual nanocavities can be identified as bright spots in the dark-field scattering image as seen in Figure 1d. The different colors of the spots represent the varying resonances of each film-coupled nanocube's associated fundamental cavity mode. The edges of the monolayer MoS_2 flake appear as blue outlines due to light scattering. For enhanced PL measurements, a defocused laser beam of ~20 μm is used for illumination to identify the individual nanocavities that are resonant with the intrinsic PL emission spectrum, which appear as bright diffraction-limited spots compared with the weak emission from the surrounding MoS_2 monolayer flake. We then obtain white-light scattering spectra of individual nanocavities in order to determine their exact plasmon resonance. Once the obtained single cavity scattering spectrum overlaps with either the A or B exciton peak (Figure 2), a diffraction-limited laser spot (~350 nm diameter) is used to excite individual nanocavities, and the PL is collected by an imaging spectrograph (see Optical Measurements).

Typically, a plasmonic nanocavity with a 10 nm spacer layer, consisting of 5 nm Al_2O_3 layer, a MoS_2 monolayer, 1 nm adhesion layer and 3 nm PVP coating, combined with a 75 nm nanocube leads to a resonant wavelength of ~650 nm, which is around the intrinsic A exciton emission peak (663 nm), as observed on the native thermal oxide SiO_2 (300 nm)/Si substrate.[34,36] Likewise, a nanocavity with a 10 nm spacer layer and a 65 nm nanocube has a resonant wavelength of ~620 nm, close to the intrinsic B exciton peak (616 nm).[34,36] Additionally, a previous PL excitation study has shown that the largest enhancement factor occurs at an excitation wavelength of 420 nm,[19] which overlaps with the second-order mode of the plasmonic nanocavity and hence results in enhanced absorption. Thus, we have used the same excitation wavelength of 420 nm for all of the PL measurements in this work.

At 420 nm excitation, a nanocavity with a plasmon resonance at 676 nm exhibits a 53-fold enhancement in the A exciton peak intensity and a 7-fold enhancement in the B exciton peak intensity (Figure 2a). The enhancement factors here refer to the ratio of the fitted A or B exciton peak intensities from the nanocavity sample (red curve) to the control sample (black curve) at the same excitation power and using the same diffraction-limited laser spot, which are not normalized to the area under a single nanocube. The white-light scattering spectrum for this particular nanocavity is also displayed in Figure 2a (blue curve). Its fundamental mode at 676 nm shows a good overlap with the A exciton peak, thus mostly enhancing the A exciton peak intensity. Likewise, a nanocavity with a plasmon resonance at 611 nm (blue curve) is resonant with the
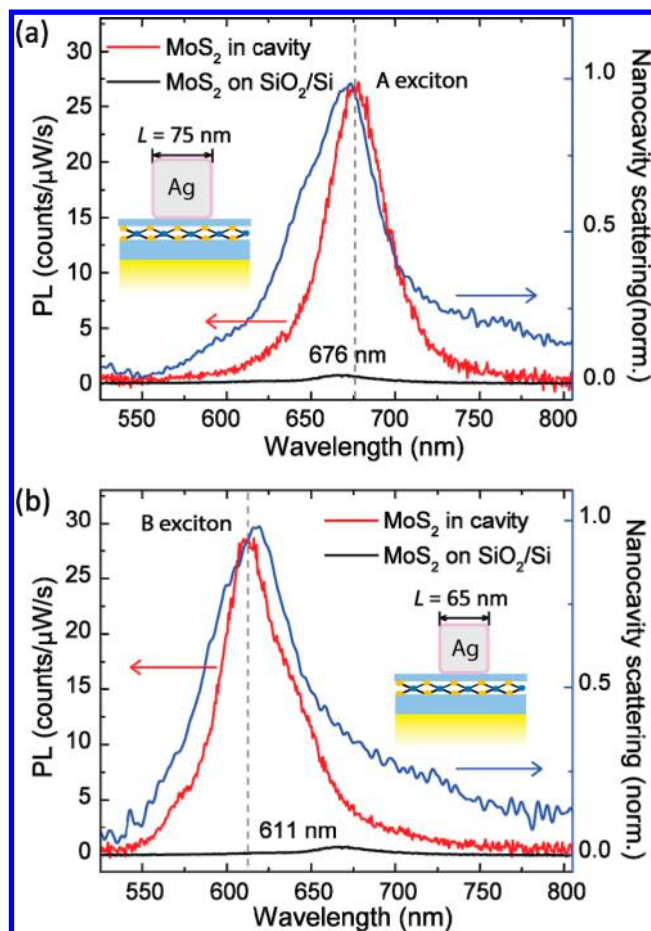
Figure 2. Selective enhancement of A and B exciton emission. (a) PL spectra from a MoS_2 monolayer on SiO_2/Si (black) and a MoS_2 monolayer in the nanocavity containing a 75 nm nanocube (red), mostly enhancing the A exciton emission peak (vertical dashed line). The measured dark-field scattering spectrum of this nanocavity is shown in the blue curve. (b) PL spectra from a MoS_2 monolayer on SiO_2/Si (black) and a MoS_2 monolayer in the nanocavity containing a 65 nm nanocube (red), mostly enhancing the B exciton emission peak (vertical dashed line). The measured dark-field scattering spectrum of this nanocavity is shown in the blue curve.

B exciton peak, as shown in Figure 2b. Consequently, a 211-fold enhancement in the B exciton peak intensity is observed while the A exciton peak intensity exhibits a 17-fold enhancement relative to the control sample (Figure 2b).

In addition to the enhancements in the peak intensities, the shape, and particularly the positions, of both emission peaks are strongly modified by the nanocavity. Notably, a dominant B exciton peak is observed in Figure 2b, which is in stark contrast to the intrinsic PL spectrum of monolayer MoS_2, which features a strongly dominating A exciton emission (Figure 1a). Additionally, from Figure 2 it is seen that coupling monolayer MoS_2 to these plasmonic nanocavities causes the emission peaks to be tuned toward the cavity resonance.

Next, we explore how far the emission peaks can be tuned from their intrinsic values and the effect of varying the nanocavity resonance on the A and B exciton emission spectra. To reveal the effect of the nanocavity resonance on the shifted PL emission peaks, we investigate the PL spectrum at a number of cavity resonances using three different batches of nanocubes with an average nanocube size of 50 nm, 65 and 75 nm. The distribution of the nanocube edge lengths L in each batch
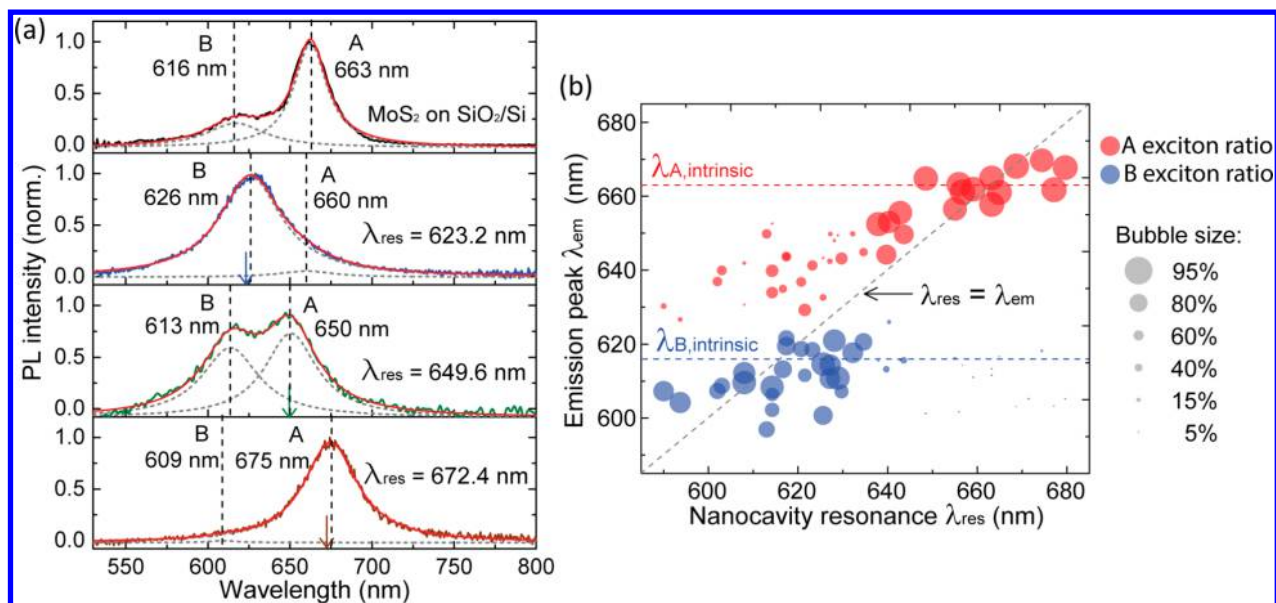
Figure 3. Modification of monolayer MoS_2 emission spectrum. (a) Shifted PL emission peaks relative to the control sample when monolayer MoS_2 is coupled to nanocavities with varying resonances. The plasmon resonance (λ_{res}) for each individual nanocavity is indicated by the arrow in each panel. Each PL spectrum is fitted to two Lorentz-shaped peaks (dashed gray lines), correlating to the A (at lower energy) and B (at higher energy) exciton peaks. The top panel is a measured PL spectrum of a MoS_2 monolayer on the SiO_2/Si substrate as a reference. (b) Plots of the fitted emission peak wavelength (λ_{em}) for both A and B exciton peaks as a function of the nanocavity resonance (λ_{res}). The bubble size relates to the ratio of the A or B exciton peaks intensity to the overall intensities. The positions of A ($\lambda_{A,intrinsic}$) and B ($\lambda_{B,intrinsic}$) exciton peaks from the control sample is labeled by the red and blue dashed lines, respectively. The dashed gray curve shows where $\lambda_{em} = \lambda_{res}$.

allows us to investigate a wide range of nanocavity resonances across the emission spectrum from 590 to 680 nm. The shape of the emission spectrum is observed to be strongly modified by the nanocavity (Figure 3). Depending on the plasmon resonance, λ_{res}, the PL spectrum exhibits a dominant A exciton peak, a dominant B exciton peak, or both exciton peaks, as displayed in the different panels in Figure 3a. The intrinsic PL emission spectrum from the control sample is shown in the top panel for comparison.

To explore the shift of the A and B exciton peaks individually, all the PL spectra are fitted to two Lorentz-shaped peaks (dashed gray lines in Figure 3a). We regard the fitted peak with lower energy as the A exciton peak and the peak with higher energy as the B exciton peak. The extracted peak emission wavelengths, λ_{em}, for the A and B excitons are shown as a function of the nanocavity resonance, λ_{res}, in Figure 3b. The bubble size indicates the ratio of the A or B exciton peak intensity to the overall intensities, which are $I_A/(I_A + I_B)$ for the red data points and $I_B/(I_A + I_B)$ for the blue data points. By tuning the nanocavity resonance from 590 to 680 nm, most data points appear around the dashed gray line that represents $\lambda_{em} = \lambda_{res}$, which indicates that the emission peak wavelengths of both the A and B excitons closely follow the nanocavity resonance. The A exciton peak shifts over 40 nm while the B exciton peak exhibits a 25 nm shift relative to the intrinsic emission wavelengths. While the intrinsic A and B exciton energies are not modified by the nanocavity, the nanocavity enhances different parts of the broad room temperature emission peaks depending on the plasmon resonance, thus resulting in a relative shift in both emission peaks.

Next, to reveal the effect of the nanocavity resonance on the PL enhancement of the A and B exciton peaks we examine the fitted peak intensities as a function of the nanocavity resonance in the range of 590 to 680 nm. From full-wave simulations,[33−35] the field enhancements depend on the lateral position of the

emitter under a single nanocube, with the largest enhancements near the corners of the nanocubes. Thus, in order to quantitatively estimate the enhancement, we define the average PL enhancement factor for a single nanocavity as[19]

$$\left\langle \text{EF} \right\rangle = \frac{I_{cav}}{I_0} \frac{A_{spot}}{A_{cav}} \tag{1}$$

where I_{cav} and I_0 are the PL intensities of the A or B exciton peaks in the cavity and from the control sample, respectively, which are obtained from the Lorentzian peak fits. The enhancement factor is also scaled to the ratio of the diffraction-limited excitation laser spot size $A_{spot} \sim (350 \text{ nm})^2$ to the area under an individual nanocube $A_{cav} \sim L^2$, where L is the nanocube edge length as labeled in Figure 1c. Thus, $\langle \text{EF} \rangle$ gives the average enhancement in PL per unit area of MoS_2 monolayer. To obtain plasmon resonances that span the entire emission spectrum, three different batches of nanocubes are used in the experiments, with average nanocube sizes of 50, 65, and 75 nm. Hence, a different value of L is used to calculate the enhancement factor $\langle \text{EF} \rangle$ for individual nanocavities depending on the specific batch of nanocubes that is addressed.

By varying the nanocavity resonance across the emission spectrum, the average enhancement factor $\langle \text{EF} \rangle$, as defined in eq 1, exhibits a strong correlation with the nanocavity resonance for both the A and B exciton peaks, as shown in Figure 4. Although all the nanocavities have the same gap thickness of ~10 nm, the measured PL intensities for the A and B exciton peaks vary from near background levels to enhancements of more than 3 orders of magnitude. In particular, the largest enhancement factors for both peaks occur at the nanocavity resonances that are slightly red-shifted relative to their intrinsic emission peaks from the control sample. The maximum enhancement of $\langle \text{EF} \rangle = 1200$ for the A exciton peak occurs at a nanocavity resonance of $\lambda_{res} = 670$ nm
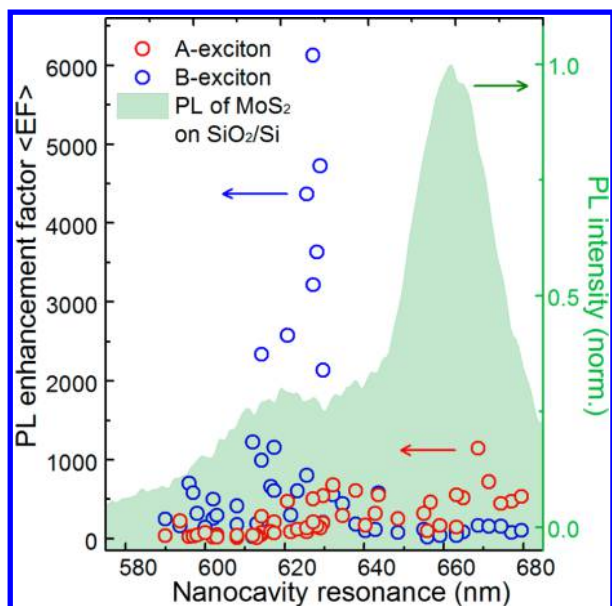
Figure 4. Relationship between PL enhancement factor and nanocavity resonance. The circles represent the PL enhancement factor ⟨EF⟩ for individual nanocavities, which is normalized to the area under a single nanocube as defined in eq 1, as a function of the nanocavity resonance for both A (red) and B (blue) exciton peaks. The highest enhancement factor is 6100-fold for the B exciton peak and 1200-fold for the A exciton peak. The normalized PL spectrum of a MoS$_2$ monolayer on the SiO$_2$/Si substrate is shown in the shaded green area.

(665 nm for the intrinsic A exciton), while the maximum enhancement of ⟨EF⟩ = 6,100 for the B exciton peak occurs at λ_{res} = 625 nm (616 nm for the intrinsic B exciton). In contrast to the factors mentioned in Figure 2, these enhancement factors are normalized to the area under an individual nanocube. As can be seen, when the nanocavity is resonant with the B exciton peak, we can enhance the inherently weak B exciton emission significantly such that the B exciton peak dominants the overall PL spectrum of monolayer MoS$_2$. This large B exciton emission is attributed to the intrinsically low quantum yield of that state. When coupled to the nanocavity, the final quantum yield of the A and B exciton emission is determined by the radiative efficiency of the nanocavity, which has previously been found to be ~50%.[34] Since the intrinsic PL peak intensity of the A exciton is about 5 times that of the B exciton peak (Figure 1a), a ~5 times larger enhancement factor is expected for the B exciton emission relative to the A exciton emission, which has been observed in our experiment (Figure 4).

In conclusion, we have demonstrated strong modification of the A and B exciton peak wavelengths by tuning the plasmonic nanocavity resonance across the emission spectrum of monolayer MoS$_2$. For the first time, we observe a dominant B exciton peak in the PL emission spectrum of monolayer MoS$_2$ when the nanocavity is resonant with the B exciton. Additionally, the PL enhancement factors for both A and B exciton peaks exhibit a strong correlation with the resonance wavelength of the fundamental mode of the nanocavity. We have observed a maximum enhancement factor of 6100-fold for the intrinsically weak B exciton peak and a maximum enhancement factor of 1200-fold for the A exciton peak. This larger enhancement factor for the B exciton emission is primarily attributed to the lower intrinsic quantum yield of the

B exciton state compared to the A exciton state. Efficient light coupling and the tunability of emission peaks in these low-dimensional nanoscale materials may facilitate highly efficient optoelectronic devices such as photodetectors, light-emitting diodes and photovoltaics. Moreover, benefiting from the colloidal fabrication technique, our observations may lead to the design of large-scale[36,38] and inexpensive nanophotonic devices with more efficient and tunable excitonic emissions.

■ SAMPLE PREPARATION

First, a 75 nm gold film was deposited onto a silicon substrate using electron beam evaporation at a deposition rate of 2 Å/s with 5 nm of chromium as an adhesion layer. Then, 5 nm of Al$_2$O$_3$ layer was deposited on the gold film via atomic layer deposition (ALD), acting as the dielectric spacer layer. Monolayer MoS$_2$ was synthesized using a seed-promoter-assisted chemical vapor deposition (CVD) method,[39] which was nucleated with the assistance of the seeding promoter perylene-3,4,9,10-tetracarboxylic acid tetrapotassium salt (PTAS). After monolayer MoS$_2$ flakes were obtained on the substrate, they were transferred to the Al$_2$O$_3$-coated gold film using a polydimethylsiloxane (PDMS) stamping method.[40] 2 μL of DI water was drop casted onto a 2 mm thick PDMS stamp, and the droplet was pressed against the MoS$_2$ on the growth substrate. Then, the PDMS stamp was peeled off with the MoS$_2$ attached and was subsequently pressed against the Al$_2$O$_3$-coated gold film. After the PDMS stamp was peeled off, monolayer MoS$_2$ was left behind on the top surface of the Al$_2$O$_3$ layer.

Next, 10 μL of cationic poly(allylamine) hydrochloride (PAH; 3 mM) droplet was deposited using a micropipette onto a region of the substrate that contained MoS$_2$ monolayers. After 5 min, the droplet was removed using the micropipette, followed by several washes with 10 μL of DI water droplets. The silver nanocubes were synthesized by Nanocomposix, Inc. (San Diego) in sizes ranging from 50 to 75 nm. After a 1000-fold dilution, a 5 μL droplet of the nanocube solution was deposited onto the region coated with PAH layer, to which the nanocubes adhered. After 15 min, the nanocube droplet was removed using a micropipette, followed by several washes with 10 μL of water droplets.

■ OPTICAL MEASUREMENTS

All of the optical measurements were performed using a custom-built bright-field/dark-field confocal microscope. Individual nanocavities and monolayer MoS$_2$ crystals were first identified under dark-field illumination imaging using a 100×, 0.9 NA dark-field microscope objective. In order to identify the plasmon resonance wavelength, the white-light scattering spectrum of individual nanocavities was obtained by a HR550 Horiba Jobin Yvon spectrometer and Symphony charge coupled device (CCD) camera. A pinhole aperture was placed at the intermediate image plane to select the scattered light from individual nanocavities. The excitation source for the PL measurements was a 420 nm pulsed laser from a frequency-doubled Ti:sapphire laser with a 150 fs pulse length and an 80 MHz repetition rate. The output of the Ti:sapphire laser was coupled to a single-mode fiber. The collimated fiber output was then defocused to a ~20 μm diameter laser spot and imaged on the sample plane through the objective. The fluorescence image was collected using the same objective and imaged on an electron multiplying digital camera (Hamamatsu EM-CCD,

model C9100). We then only selected nanocavities that exhibited enhanced PL under this wide-field excitation and also possessed a plasmon resonance in the range of 590 to 680 nm, as determined from the dark-field scattering spectrum. For measurements of PL enhancements, the defocusing lens was removed and the laser was focused on the individual nanocavity to a diffraction-limited spot with a diameter of ∼350 nm. The PL of monolayer MoS_2 on gold in areas far from the nanocavity was very weak and contributed <10% of the total PL signal. The PL was then collected by the objective, passed through a 550 nm long-pass filter (Omega Optics) and detected by the imaging spectrograph.

■ AUTHOR INFORMATION

Corresponding Author
*E-mail: m.mikkelsen@duke.edu.

ORCID ◉
Maiken H. Mikkelsen: 0000-0002-0487-7585

Author Contributions
J.H. and G.M.A. performed the experiments and data analysis. T.M. and J.K. fabricated the monolayer MoS_2 samples. J.H. and G.M.A. fabricated the nanocavity samples. J.H. and M.H.M. wrote the manuscript with input from all coauthors. M.H.M. designed and supervised the project.

Notes
The authors declare no competing financial interest.

■ REFERENCES

(1) Wang, Q. H.; Kalantar-Zadeh, K.; Kis, A.; Coleman, J. N.; Strano, M. S. Electronics and Optoelectronics of Two-Dimensional Transition Metal Dichalcogenides. *Nat. Nanotechnol.* **2012**, *7*, 699−712.

(2) Mak, K. F.; Lee, C.; Hone, J.; Shan, J.; Heinz, T. F. Atomically Thin MoS_2: A New Direct-Gap Semiconductor. *Phys. Rev. Lett.* **2010**, *105*, 136805.

(3) Prins, F.; Goodman, A. J.; Tisdale, W. A. Reduced Dielectric Screening and Enhanced Energy Transfer in Single- and Few-Layer MoS_2. *Nano Lett.* **2014**, *14*, 6087−6091.

(4) Goodfellow, K. M.; Beams, R.; Chakraborty, C.; Novotny, L.; Vamivakas, A. N. Integrated Nanophotonics Based on Nanowire Plasmons and Atomically Thin Material. *Optica* **2014**, *1*, 149−152.

(5) Lee, H. S.; Kim, M. S.; Jin, Y.; Han, G. H.; Lee, Y. H.; Kim, J. Selective Amplification of the Primary Exciton in a MoS_2 Monolayer. *Phys. Rev. Lett.* **2015**, *115*, 226801.

(6) Geim, A. K.; Grigorieva, I. V. Van Der Waals Heterostructures. *Nature* **2013**, *499*, 419−425.

(7) Rigosi, A. F.; Hill, H. M.; Li, Y.; Chernikov, A.; Heinz, T. F. Probing Interlayer Interactions in Transition Metal Dichalcogenide Heterostructures by Optical Spectroscopy: MoS_2/WS_2 and $MoSe_2/WSe_2$. *Nano Lett.* **2015**, *15*, 5033−5038.

(8) He, K.; Kumar, N.; Zhao, L.; Wang, Z.; Mak, K. F.; Zhao, H.; Shan, J. Tightly Bound Excitons in Monolayer WSe_2. *Phys. Rev. Lett.* **2014**, *113*, 26803.

(9) Shi, H.; Yan, R.; Bertolazzi, S.; Brivio, J.; Gao, B.; Kis, A.; Jena, D.; Xing, H. G.; Huang, L. Exciton Dynamics in Suspended MoS_2 Monolayer. *ACS Nano* **2013**, *7*, 1072−1080.

(10) Zeng, H.; Dai, J.; Yao, W.; Xiao, D.; Cui, X. Valley Polarization in MoS_2 Monolayers by Optical Pumping. *Nat. Nanotechnol.* **2012**, *7*, 490−493.

(11) Mak, K. F.; He, K. L.; Shan, J.; Heinz, T. F. Control of Valley Polarization in Monolayer MoS_2 by Optical Helicity. *Nat. Nanotechnol.* **2012**, *7*, 494−498.

(12) Wang, Q.; Ge, S.; Li, X.; Qiu, J.; Ji, Y.; Feng, J.; Sun, D. Valley Carrier Dynamics in Monolayer Molybdenum Disulfide from Helicity-Resolved Ultrafast Pump-Probe Spectroscopy. *ACS Nano* **2013**, *7*, 11087−11093.

(13) Sim, S.; Park, J.; Song, J. G.; In, C.; Lee, Y. S.; Kim, H.; Choi, H. Exciton Dynamics in Atomically Thin MoS_2: Interexcitonic Interaction and Broadening Kinetics. *Phys. Rev. B* **2013**, *88*, 75434.

(14) Sun, D.; Rao, Y.; Reider, G. A.; Chen, G.; You, Y.; Brezin, L.; Harutyunyan, A. R.; Heinz, T. F. Observation of Rapid Exciton − Exciton Annihilation in Monolayer Molybdenum Disulfide. *Nano Lett.* **2014**, *14*, 5625−5629.

(15) Lagarde, D.; Bouet, L.; Marie, X.; Zhu, C. R.; Liu, B. L.; Amand, T.; Tan, P. H.; Urbaszek, B. Carrier and Polarization Dynamics in Monolayer MoS_2. *Phys. Rev. Lett.* **2014**, *112*, 47401.

(16) Wang, H.; Zhang, C.; Rana, F. Ultrafast Dynamics of Defect-Assisted Electron−Hole Recombination in Monolayer MoS_2. *Nano Lett.* **2015**, *15*, 339−345.

(17) Huang, J.; Hoang, T. B.; Mikkelsen, M. H. Probing the Origin of Excitonic States in Monolayer WSe_2. *Sci. Rep.* **2016**, *6*, 22414.

(18) Xiao, D.; Liu, G. B.; Feng, W. X.; Xu, X. D.; Yao, W. Coupled Spin and Valley Physics in Monolayers of MoS_2 and Other Group-VI Dichalcogenides. *Phys. Rev. Lett.* **2012**, *108*, 196802.

(19) Akselrod, G. M.; Ming, T.; Argyropoulos, C.; Hoang, T. B.; Lin, Y.; Ling, X.; Smith, D. R.; Kong, J.; Mikkelsen, M. H. Leveraging Nanocavity Harmonics for Control of Optical Processes in 2D Semiconductors. *Nano Lett.* **2015**, *15*, 3578−3584.

(20) Najmaei, S.; Mlayah, A.; Arbouet, A.; Girard, C.; Leotin, J.; Lou, J. Plasmonic Pumping of Excitonic Photoluminescence in Hybrid MoS_2-Au Nanostructures. *ACS Nano* **2014**, *8*, 12682−12689.

(21) Sobhani, A.; Lauchner, A.; Najmaei, S.; Ayala-Orozco, C.; Wen, F.; Lou, J.; Halas, N. J. Enhancing the Photocurrent and Photo-luminescence of Single Crystal Monolayer MoS_2 with Resonant Plasmonic Nanoshells. *Appl. Phys. Lett.* **2014**, *104*, 31112.

(22) Butun, S.; Tongay, S.; Aydin, K. Enhanced Light Emission from Large-Area Monolayer MoS_2 Using Plasmonic Nanodisc Arrays. *Nano Lett.* **2015**, *15* (4), 2700−2704.

(23) Lee, B.; Park, J.; Han, G. H.; Ee, H. S.; Naylor, C. H.; Liu, W.; Johnson, A. T. C.; Agarwal, R. Fano Resonance and Spectrally Modified Photoluminescence Enhancement in Monolayer MoS_2 Integrated with Plasmonic Nanoantenna Array. *Nano Lett.* **2015**, *15*, 3646−3653.

(24) Kern, J.; Trugler, A.; Niehues, I.; Ewering, J.; Schmidt, R.; Schneider, R.; Najmaei, S.; George, A.; Zhang, J.; Lou, J.; Hohenester, U.; Michaelis De Vasconcellos, S.; Bratschitsch, R. Nanoantenna-Enhanced Light-Matter Interaction in Atomically Thin WS_2. *ACS Photonics* **2015**, *2*, 1260−1265.

(25) Lee, K. C. J.; Chen, Y.-H.; Lin, H.-Y.; Cheng, C.-C.; Chen, P.-Y.; Wu, T.-Y.; Shih, M.-H.; Wei, K.-H.; Li, L.-J.; Chang, C.-W. Plasmonic Gold Nanorods Coverage Influence on Enhancement of the Photoluminescence of Two-Dimensional MoS_2 Monolayer. *Sci. Rep.* **2015**, *5*, 16374.

(26) Gao, W.; Lee, Y. H.; Jiang, R.; Wang, J.; Liu, T.; Ling, X. Y. Localized and Continuous Tuning of Monolayer MoS_2 Photo-luminescence Using a Single Shape-Controlled Ag Nanoantenna. *Adv. Mater.* **2016**, *28*, 701−706.

(27) Zhu, Y.; Yang, J.; Zhang, S.; Mokhtar, S.; Pei, J.; Wang, X.; Lu, Y. Strongly Enhanced Photoluminescence in Nanostructured Monolayer

MoS$_2$ by Chemical Vapor Deposition. *Nanotechnology* **2016**, *27*, 135706.

(28) Chen, H.; Yang, J.; Rusak, E.; Straubel, J.; Guo, R.; Myint, Y. W.; Pei, J.; Decker, M.; Staude, I.; Rockstuhl, C.; Lu, Y.; Kivshar, Y. S.; Neshev, D. Manipulation of Photoluminescence of Two-Dimensional MoSe$_2$ by Gold Nanoantennas. *Sci. Rep.* **2016**, *6*, 22296.

(29) Amani, M.; Lien, D.-H.; Kiriya, D.; Xiao, J.; Azcatl, A.; Noh, J.; Madhvapathy, S. R.; Addou, R.; KC, S.; Dubey, M.; Cho, K.; Wallace, R. M.; Lee, S.-C.; He, J.-H.; Ager, J. W.; Zhang, X.; Yablonovitch, E.; Javey, A. Near-Unity Photoluminescence Quantum Yield in MoS$_2$. *Science* **2015**, *350*, 1065−1068.

(30) Wu, S.; Buckley, S.; Jones, A. M.; Ross, J. S.; Ghimire, N. J.; Yan, J.; Mandrus, D. G.; Yao, W.; Hatami, F.; Vučković, J.; Majumdar, A.; Xu, X. Control of Two-Dimensional Excitonic Light Emission via Photonic Crystal. *2D Mater.* **2014**, *1* (1), 11001.

(31) Ding, S.-Y.; Yi, J.; Li, J.-F.; Ren, B.; Wu, D.-Y.; Panneerselvam, R.; Tian, Z.-Q. Nanostructure-Based Plasmon-Enhanced Raman Spectroscopy for Surface Analysis of Materials. *Nat. Rev. Mater.* **2016**, *1*, 16021.

(32) Lassiter, J. B.; Chen, X.; Liu, X.; Ciracì, C.; Hoang, T. B.; Larouche, S.; Oh, S.-H.; Mikkelsen, M. H.; Smith, D. R. Third-Harmonic Generation Enhancement by Film-Coupled Plasmonic Stripe Resonators. *ACS Photonics* **2014**, *1*, 1212−1217.

(33) Rose, A.; Hoang, T. B.; McGuire, F.; Mock, J. J.; Ciracì, C.; Smith, D. R.; Mikkelsen, M. H. Control of Radiative Processes Using Tunable Plasmonic Nanopatch Antennas. *Nano Lett.* **2014**, *14*, 4797−4802.

(34) Akselrod, G. M.; Argyropoulos, C.; Hoang, T. B.; Ciracì, C.; Fang, C.; Huang, J.; Smith, D. R.; Mikkelsen, M. H. Probing the Mechanisms of Large Purcell Enhancement in Plasmonic Nano-antennas. *Nat. Photonics* **2014**, *8* (11), 835−840.

(35) Hoang, T. B.; Akselrod, G. M.; Argyropoulos, C.; Huang, J.; Smith, D. R.; Mikkelsen, M. H. Ultrafast Spontaneous Emission Source Using Plasmonic Nanoantennas. *Nat. Commun.* **2015**, *6*, 7788.

(36) Akselrod, G. M.; Huang, J.; Hoang, T. B.; Bowen, P. T.; Su, L.; Smith, D. R.; Mikkelsen, M. H. Large-Area Metasurface Perfect Absorbers from Visible to Near-Infrared. *Adv. Mater.* **2015**, *27*, 8028.

(37) Mak, K. F.; He, K. L.; Lee, C.; Lee, G. H.; Hone, J.; Heinz, T. F.; Shan, J. Tightly Bound Trions in Monolayer MoS$_2$. *Nat. Mater.* **2012**, *12*, 207−211.

(38) Stewart, J. W.; Akselrod, G. M.; Smith, D. R.; Mikkelsen, M. H. Toward Multispectral Imaging with Colloidal Metasurface Pixels. *Adv. Mater.* **2017**, *29* (6), 1602971.

(39) Ling, X.; Lee, Y.-H.; Lin, Y.; Fang, W.; Yu, L.; Dresselhaus, M. S.; Kong, J. Role of the Seeding Promoter in MoS$_2$ Growth by Chemical Vapor Deposition. *Nano Lett.* **2014**, *14*, 464−472.

(40) Lee, Y.; Yu, L.; Wang, H.; Fang, W.; Ling, X.; Shi, Y.; Lin, C.; Huang, J.; Chang, M.; Chang, C.; Dresselhaus, M.; Palacios, T.; Li, L.; Kong, J. Synthesis and Transfer of Single-Layer Transition Metal Disulfides on Diverse Surfaces. *Nano Lett.* **2013**, *13*, 1852−1857.